bioRxiv preprint doi: https://doi.org/10.1101/2020.09.16.299305; this version posted September 16, 2020. The copyright holder for this preprint (which was not certified by peer review) is the author/funder, who has granted bioRxiv a license to display the preprint in perpetuity. It is made available under aCC-BY-NC-ND 4.0 International license.

Mean-field modeling of brain-scale dynamics for the evaluation of EEG source-space networks

Sahar Allouch[1,2], Maxime Yochum[1], Aya Kabbara[1], Joan Duprez[1], Mohamad Khalil[2,4], Fabrice Wendling[1], Mahmoud Hassan[3], Julien Modolo[1]

[1] Univ Rennes, LTSI - INSERM U1099, F-35000 Rennes, France

[2] Azm Center for Research in Biotechnology and Its Applications, EDST, Tripoli, Lebanon.

[3] NeuroKyma, F-35000 Rennes, France

[4] CRSI research center, Faculty of Engineering, Lebanese University, Beirut, Lebanon

Corresponding author: Sahar Allouch, saharallouch@gmail.com

bioRxiv preprint doi: https://doi.org/10.1101/2020.09.16.299305; this version posted September 16, 2020. The copyright holder for this preprint (which was not certified by peer review) is the author/funder, who has granted bioRxiv a license to display the preprint in perpetuity. It is made available under aCC-BY-NC-ND 4.0 International license.

Abstract

Understanding the dynamics of brain-scale functional networks at rest and during cognitive tasks is the subject of intense research efforts to unveil fundamental principles of brain functions. To estimate these large-scale brain networks, the emergent method called "electroencephalography (EEG) source connectivity" has generated increasing interest in the network neuroscience community, due to its ability to identify cortical brain networks with good spatio-temporal resolution, while reducing mixing and volume conduction effects. However, the method is still immature and several methodological issues should be carefully accounted for to avoid pitfalls. Therefore, optimizing the EEG source connectivity pipelines is required, which involves the evaluation of several parameters. One key issue to address those evaluation aspects is the availability of a 'ground truth'. In this paper, we show how a recently developed large-scale model of brain-scale activity, named COALIA, can provide to some extent such ground truth by providing realistic simulations (epileptiform activity) of source-level and scalp-level activity. Using a bottom-up approach, the model bridges cortical micro-circuitry and large-scale network dynamics. Here, we provide an example of the potential use of COALIA to analyze the effect of three key factors involved in the "EEG source connectivity" pipeline: (i) EEG sensors density, (ii) algorithm used to solve the inverse problem, and (iii) functional connectivity measure. Results show that a high electrode density (at least 64 channels) is needed to accurately estimate cortical networks. Regarding the inverse solution/connectivity measure combination, the best performance at high electrode density was obtained using the weighted minimum norm estimate (wMNE) combined with the weighted phase lag index (wPLI). The COALIA model and the simulations used in this paper are freely available and made accessible for the community. We believe that this model-based approach will help researchers to address some current and future

bioRxiv preprint doi: https://doi.org/10.1101/2020.09.16.299305; this version posted September 16, 2020. The copyright holder for this preprint (which was not certified by peer review) is the author/funder, who has granted bioRxiv a license to display the preprint in perpetuity. It is made available under aCC-BY-NC-ND 4.0 International license.

cognitive and clinical neuroscience questions, and ultimately transform EEG brain network imaging into a mature technology.

Keywords: neural mass models, electroencephalography, EEG sensor density, inverse problem, functional connectivity, network neuroscience.

bioRxiv preprint doi: https://doi.org/10.1101/2020.09.16.299305; this version posted September 16, 2020. The copyright holder for this preprint (which was not certified by peer review) is the author/funder, who has granted bioRxiv a license to display the preprint in perpetuity. It is made available under aCC-BY-NC-ND 4.0 International license.

Introduction

There is now growing evidence suggesting that large-scale functional brain networks underlie complex brain functions during rest (Allen et al., 2014; Kabbara et al., 2017) and tasks (Hassan et al., 2015; O′Neill et al., 2016). In this context, a relatively new field called "network neuroscience" has emerged (Bassett and Sporns, 2017), offering the opportunity to assess, quantify, and ultimately understand the multifaceted features of complex brain networks. Among the neuroimaging techniques used to derive the functional brain networks, the electroencephalography (EEG) technique provides a direct measure of electrical brain activity at the millisecond time scale. The past years have seen a noticeable increase of interest in "EEG source connectivity" methods to estimate brain networks at the cortical sources level, while minimizing the volume conduction and field spread problems (Hassan and Wendling, 2018; Schoffelen and Gross, 2009). Although consisting only of two main steps: 1) the source reconstruction and 2) the connectivity assessment, there is still no consensus on a unified pipeline adapted to this approach, and many methodological questions remain unanswered. A first issue lies at the very first step of data recording with the question of optimal spatial resolution (i.e. density of sensors) needed to avoid misrepresentation of spatial information of brain activity. A second critical issue concerns the data preprocessing techniques. Regarding the subsequent analysis and for each of the aforementioned steps, a large number of methods is available, each having its own properties, advantages and drawbacks, and addressing a different aspect of the data. An additional parameter warranting investigation is the spatial resolution of the reconstructed cortical sources (i.e. number of regions of interest) ranging from dozens to thousands of regions.

bioRxiv preprint doi: https://doi.org/10.1101/2020.09.16.299305; this version posted September 16, 2020. The copyright holder for this preprint (which was not certified by peer review) is the author/funder, who has granted bioRxiv a license to display the preprint in perpetuity. It is made available under aCC-BY-NC-ND 4.0 International license.

To tackle those challenges, several comparative studies have been conducted with the aim of evaluating the performance of the adopted techniques and the influence of different parameters affecting the network estimation procedure (Anzolin et al., 2019; Colclough et al., 2016; Fornito et al., 2010; Halder et al., 2019; Lantz et al., 2003; Sohrabpour et al., 2015; Song et al., 2015; Wang et al., 2009; Zalesky et al., 2010). In the context of EEG, several studies investigated the effect of different electrode montages on the estimation of functional connectivity. Increasing the number of electrodes has been shown to decrease the localization error in different contexts (Lantz et al., 2003; Sohrabpour et al., 2015; Song et al., 2015). (Song et al., 2015) recommended using 128 or 256 electrodes, while in (Sohrabpour et al., 2015) the most dramatic decrease in localization error was obtained when going from 32 to 64 electrodes. Other studies have focused on evaluating the performance of different inverse solutions using simulated and real EEG signals (Anzolin et al., 2019; Bradley et al., 2016; Grova et al., 2006; Halder et al., 2019). Compared methods include those based on the minimum norm estimate (MNE, LORETA, sLORETA, eLORETA, etc.) as well as beamformers (DICS, LCMV). However, there is no consensus on which inverse solution provides the most accurate results when estimating EEG/MEG source-space networks. In the context of functional connectivity, the performance of various measures covering direct/indirect causal relations, marginal/partial associations, leakage correction, amplitude/phase coupling have been evaluated, and compared using either real data (Colclough et al., 2016), or simulated data in (Wang et al., 2014; Wendling et al., 2009). As for the source reconstruction algorithm, no consensus has been reached on which connectivity measure to adopt.

However, a challenging issue in such studies resides in the absence of a ‘ground truth’. Ideally, simultaneous scalp EEG and depth (intracranial) recordings are required, which is challenging to

bioRxiv preprint doi: https://doi.org/10.1101/2020.09.16.299305; this version posted September 16, 2020. The copyright holder for this preprint (which was not certified by peer review) is the author/funder, who has granted bioRxiv a license to display the preprint in perpetuity. It is made available under aCC-BY-NC-ND 4.0 International license.

perform and is therefore unavailable in most studies. Thus, to overcome this issue, one solution is to use simulated data derived from physiologically-inspired models, which is an approach followed in the present study. Here, we use a computational model named "COALIA" (Bensaid et al., 2019) able to generate realistic brain-scale, cortical-level simulations from which scalp EEG signals can be obtained through the EEG direct problem, thereby representing a ground truth for subsequent analysis. More specifically, COALIA simulates electrophysiological activity as a function of the detailed circuitry between the main neuronal subtypes and anatomical regions. We highlight the implications of this model in enhancing our interpretation of the reconstructed brain networks and in evaluating the key factors of the EEG source connectivity pipeline such as 1) EEG sensor density, 2) solution of the EEG inverse problem, and 3) functional connectivity measure.

Here, we generate epileptiform cortical activity and present a (not exhaustive) comparative study to evaluate the effect of five different electrode densities (256, 128, 64, 32, 19), two inverse solution algorithms, weighted minimum norm estimate (wMNE) and exact low resolution electromagnetic tomography (eLORETA), and two functional connectivity measures, phase locking value (PLV) and weighted minimum norm estimate (wPLI), as they represent the most used combination of methods in the context of EEG source-space network estimation. We aim at presenting a proof of concept of the interest of COALIA in the network neuroscience field, and its potential use in optimizing the EEG source-space network estimation pipeline.

Materials and Methods

The full pipeline of our study is summarized in Fig. 1.

bioRxiv preprint doi: https://doi.org/10.1101/2020.09.16.299305; this version posted September 16, 2020. The copyright holder for this preprint (which was not certified by peer review) is the author/funder, who has granted bioRxiv a license to display the preprint in perpetuity. It is made available under aCC-BY-NC-ND 4.0 International license.

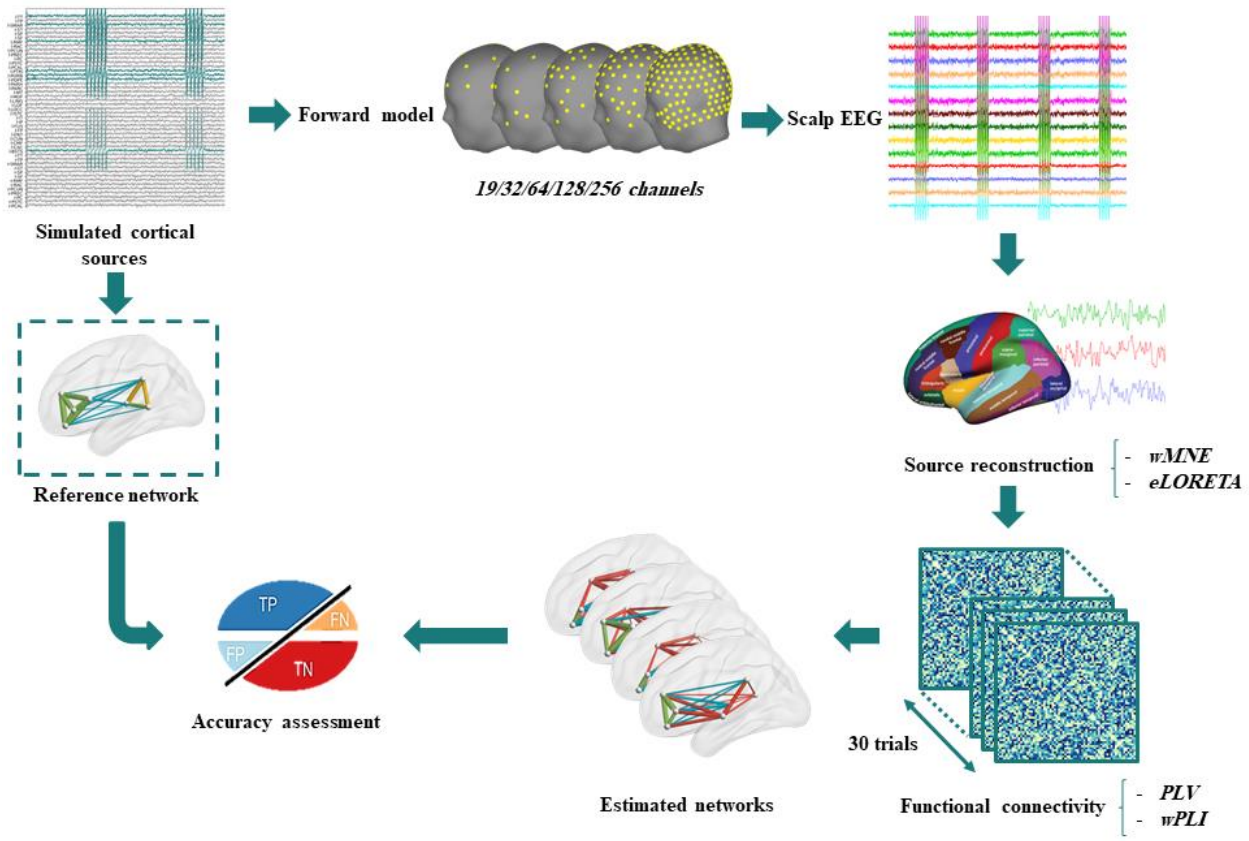

Fig. 1 Pipeline of the study. Cortical sources were simulated using COALIA. The forward model was solved for five electrode montages (19, 32, 64, 128, 256 electrodes). Scalp EEG signals were generated. Cortical sources were reconstructed using wMNE and eLORETA as inverse solutions. Functional connectivity between reconstructed sources was assessed over 30 trials using PLV and wPLI algorithms. Accuracy was computed to assess the performance of the network estimation.

COALIA: a physiologically-inspired computational model

COALIA is a recently developed physiologically-grounded computational model (Bensaid et al., 2019) of large-scale brain activity. Using a bottom-up approach taking account the detailed circuitry between the main neuronal subtypes, and anatomical regions from a widely used atlas, COALIA generates brain-scale electrophysiological activity while accounting for the macro- as well as the micro-circuitry of the brain. The basic unit of the model is the neural mass, a local network involving different neuronal types in which the electrical activity is averaged over the cells of a similar type, instead of describing individual cell dynamics as in microscopic models.

bioRxiv preprint doi: https://doi.org/10.1101/2020.09.16.299305; this version posted September 16, 2020. The copyright holder for this preprint (which was not certified by peer review) is the author/funder, who has granted bioRxiv a license to display the preprint in perpetuity. It is made available under aCC-BY-NC-ND 4.0 International license.

Therefore, the neural mass model (NMM) is a mesoscopic model describing synchronized activity in local networks in which the micro-circuitry can be taken into account. At the level of a single neural mass (approximated a specific brain region, as done in (Bensaid et al., 2019)), the model includes glutamatergic pyramidal neurons and three different types of GABAergic interneurons with physiologically-based kinetics (fast vs. slow). At the brain-scale level, each neural mass represents the local field activity of one region of the Desikan-Killiany atlas (66 regions, since the right and left insula were excluded, (Desikan et al., 2006)). Given that each neural mass simulates the activity of one specific brain region, neural masses are then synaptically connected through long-range glutamatergic projections. This neuro-inspired model can simulate both cortical and thalamic activity. In the following, a brief description of the local NMM of neocortical and thalamic activity is presented (for further details, please refer to (Bensaid et al., 2019)).

The neocortical module involved pyramidal cells (PCs) and three types of inhibitory GABAergic interneurons, namely, (1) somatic-targeting parvalbumine positive (PV+) basket cells (BC); (2) the dendritic-targeting somatostatin positive (SST) interneurons; and (3) vasoactive intestinal-peptide (VIP) expressing interneurons. BC and SST received excitatory inputs from PCs, that are reciprocally inhibited by both of them. Pyramidal collateral excitation was implemented *via* an excitatory feedback loop passed by a supplementary excitatory population (PC') analogous to PC, except that it projected only to the subpopulation PC and receives projection from PC as well. An inhibitory feedback loop was implemented to account for direct PV+/PV+ coupling through electrical gap-junctions. Communication through disinhibition was modeled by inhibitory projections first from VIP to SST, then from SST to BC. The non-specific influence from neighboring and distant populations was modeled by a Gaussian input noise corresponding

bioRxiv preprint doi: https://doi.org/10.1101/2020.09.16.299305; this version posted September 16, 2020. The copyright holder for this preprint (which was not certified by peer review) is the author/funder, who has granted bioRxiv a license to display the preprint in perpetuity. It is made available under aCC-BY-NC-ND 4.0 International license.

to an excitatory input $p_c^n(t)$ that globally described the average density of afferent action potentials. The thalamic module included one population of excitatory glutamatergic neurons (TCs, i.e. thalamic cells), and two thalamic reticular nuclei (TRN) GABAergic interneurons. TCs received GABAergic IPSPs with slow and fast kinetics from the TRNs, whereas the latter received excitatory inputs from the former. As in the cortical module, a Gaussian input noise corresponding to excitatory input $p_c^n(t)$ was used to represent non-specific inputs on TCs.

At the brain-scale, glutamatergic PCs originating from a single cortical column targeted PCs of other cortical columns by common feedforward excitation and GABAergic cells by disynaptic cortico-cortical feedforward inhibition. Variable time delays between NMMs were introduced in order to account for activity propagation delays caused by long-range connections. Regarding thalamo-cortical connectivity, TCs received glutamatergic excitatory postsynaptic potentials (EPSPs) from PCs which, in turn, received excitatory input from TCs. Similarly, TRNs received excitatory cortical projections. In terms of GABAergic cortical targets, thalamic projections targeted PV+ basket cells, SST neurons as well as VIP neurons, which in turn inhibit SST neurons, and disinhibit PCs dendrites. The model output corresponds to the total input onto PCs in the cortical modules (i.e. sum of excitatory and inhibitory PSPs).

Simulations

We considered a scenario consisting in two connected subnetworks consisting of 7 brain regions (from the Desikan-Killiany atlas) located in the left hemisphere. This simulated network was inspired from a general scheme of the organization of human partial seizures presented in (Bartolomei et al., 2013) and proposing the existence of an epileptogenic subnetwork as well as a propagation subnetwork. In the present study, the epileptogenic subnetwork included the

bioRxiv preprint doi: https://doi.org/10.1101/2020.09.16.299305; this version posted September 16, 2020. The copyright holder for this preprint (which was not certified by peer review) is the author/funder, who has granted bioRxiv a license to display the preprint in perpetuity. It is made available under aCC-BY-NC-ND 4.0 International license.

following cortical regions: rostral middle frontal gyrus, pars opercularis, pars triangularis, and pars orbitalis; and the propagation subnetwork included the supramarginal, banks superior temporal sulcus, and transverse temporal cortex. Background activity was simulated in all 66 regions while a rhythmic spike activity was imposed to the thalamic population. The latter was unidirectionally coupled to the 7 aforementioned regions with a connectivity value of 50. Spikes propagated, thus, in the desired regions such that their activity was epileptiform. Values of the model parameters corresponding to the generated background and spiking activity are provided in the GitHub repository. All sources belonging to a single patch were synchronized at a zero lag, while a delay of 30 ms was introduced between the two subnetworks to reflect the propagation of the spikes between relatively distant regions in the brain. A timeseries of ~6 min at 2048 Hz was simulated, and was segmented into 10-second epochs. A total of 30 epochs was selected for the subsequent analysis.

EEG Electrodes density and direct problem

Five different electrode montages were used to generate scalp EEG signals. We selected the GSN HydroCel EEG configuration (EGI, Electrical geodesic Inc) for the 256, 128, 64 and 32 channels density, as well as the international 10-20 system (Klem et al., 1999) for the 19 channels array. For each electrode configuration, the lead field matrix was computed for a realistic head model using the Boundary Element Method (BEM) using OpenMEEG (Alexandre Gramfort et al., 2010) implemented in the Brainstorm toolbox (Tadel et al., 2011) for Matlab (The Mathworks, USA, version 2018b). To generate EEG scalp simulations, we used only the lead field vectors reflecting the contribution of the 66 sources located at the centroid of the regions of interest - defined on the basis of the Desikan-Killiany atlas (Desikan et al., 2006) (right and left insula were excluded) - to the sensors:

bioRxiv preprint doi: https://doi.org/10.1101/2020.09.16.299305; this version posted September 16, 2020. The copyright holder for this preprint (which was not certified by peer review) is the author/funder, who has granted bioRxiv a license to display the preprint in perpetuity. It is made available under aCC-BY-NC-ND 4.0 International license.

$$X(t) = G.S(t) \tag{1}$$

where $X(t)$, $S(t)$ are the scalp EEG and cortical timeseries respectively, and G the gain matrix.

EEG inverse problem

In the following methods, solving the EEG inverse problem consists in estimating the magnitude of:

$$\hat{S}(t) = W.X(t) \tag{2}$$

Among the various algorithms proposed to solve this problem, two of the most common methods were compared here: the weighted minimum norm estimate (wMNE) and the exact low-resolution electromagnetic tomography (eLORETA).

Weighted Minimum Norm Estimate (wMNE)

The minimum norm estimate (MNE) originally proposed by (Hämäläinen and Ilmoniemi, 1994) searches for a solution that fits the measurements with a least square error. The wMNE compensates for the tendency of MNE to favor weak and surface sources:

$$W_{wMNE} = BG^T(GBG^T + \lambda C)^{-1} \tag{3}$$

where C is the noise covariance matrix, and λ is the regularization parameter computed based on the signal-to-noise ratio ($\lambda = 1/SNR$). The matrix B is a diagonal matrix built from matrix G with non-zero terms inversely proportional to the norm of lead field vectors. It adjusts the properties of the solution by reducing the bias inherent to the standard MNE solution:

bioRxiv preprint doi: https://doi.org/10.1101/2020.09.16.299305; this version posted September 16, 2020. The copyright holder for this preprint (which was not certified by peer review) is the author/funder, who has granted bioRxiv a license to display the preprint in perpetuity. It is made available under aCC-BY-NC-ND 4.0 International license.

$$B_{ij} = \begin{cases} (G_i^T G_i)^{1/2} & if\ i = j \\ 0 & if\ i \neq j \end{cases} \tag{4}$$

Exact low-resolution brain electromagnetic tomography (eLORETA)

The exact low-resolution electromagnetic tomography (eLORETA) belongs to the family of the weighted minimum norm inverse solution. However, it does not only account for depth bias, it has, also, exact zero error localization in the presence of measurement and structured biological noise (Pascual-Marqui, 2007).

$$B_{ij} = \begin{cases} (G_i^T (G_i B G_i^T + \lambda C)^{-1} G_i)^{1/2} & if\ i = j \\ 0 & if\ i \neq j \end{cases} \tag{5}$$

eLORETA is originally described using the whole brain volume as source space. However, in the present study, in order to facilitate the comparison with other methods, we restricted the source space to the cortical surface.

Connectivity measures

We evaluated in this study two of the most popular connectivity metrics, both based on the assessment of the phase synchrony between regional time-courses.

Phase-locking value

For two signals $x(t)$ and $y(t)$, the phase-locking value (Lachaux et al., 2000) is defined as:

$$PLV = \left| E\{e^{i|\varphi_x(t) - \varphi_y(t)|}\} \right| \tag{6}$$

bioRxiv preprint doi: https://doi.org/10.1101/2020.09.16.299305; this version posted September 16, 2020. The copyright holder for this preprint (which was not certified by peer review) is the author/funder, who has granted bioRxiv a license to display the preprint in perpetuity. It is made available under aCC-BY-NC-ND 4.0 International license.

where $E\{\,.\,\}$ is the expected value operator and $\varphi(t)$ is the instantaneous phase derived from the Hilbert transform.

Weighted phase-lag index

While the phase-lag index (PLI) quantifies the asymmetry of the phase difference, rendering it insensitive to shared signals at zero phase lag (Stam et al., 2007) that supposedly induce spurious volume conduction effects, the weighted PLI (wPLI) attempts to further weight the metric away from zero-lag contributions (Vinck et al., 2011).

$$wPLI = \frac{|E\{|\Im\{X\}|\ sign(\Im\{X\})\}|}{E\{|\Im\{X\}|\}} \tag{7}$$

where $\Im\{X\}$ denotes the imaginary part of the signal's cross-spectrum.

Connectivity matrices were computed in broadband [1-45 Hz] for all considered electrode densities and possible inverse solution/connectivity combinations, resulting in 20 connectivity matrices for each epoch. The resulting matrices were thresholded by keeping nodes with the highest 12% strength values, which corresponds to the proportion of nodes originally used to simulate the 2 subnetworks. A node's strength was defined as the sum of the weights of its corresponding edges.

Results quantification

In order to assess the performance of each investigated parameter (i.e. electrodes number, inverse solution, connectivity measure), the accuracy of the estimated networks with respect to the ground truth was computed as follows:

bioRxiv preprint doi: https://doi.org/10.1101/2020.09.16.299305; this version posted September 16, 2020. The copyright holder for this preprint (which was not certified by peer review) is the author/funder, who has granted bioRxiv a license to display the preprint in perpetuity. It is made available under aCC-BY-NC-ND 4.0 International license.

$$accuracy = \frac{TP + TN}{TP + TN + FP + FN} \tag{8}$$

where TP (i.e. true positive) represents the connections present in the reference as well as in the estimated network, TN (i.e. true negative) refers to the absent connections in both the reference and estimated networks, FP (i.e. false positive) represents the connections obtained in the estimated network exclusively, and FN stands for the links missing in the estimated network. Accuracy values range between 0 and 1.

Statistical analysis

Statistical analyses were performed using R (R Core Team, 2020). We used linear mixed model analyses to investigate the effects of electrode number, inverse solution method, and connectivity measure on the accuracy of the estimated networks. Mixed models have several advantages, such as the ability to account for the dependence between the different measures, and to model random effects (see (Gueorguieva and Krystal, 2004)). We used the *lmer* function of the {*lme4*} package (Bates et al., 2015) with the following model that includes, epoch, electrode number, inverse solution method and connectivity measures as interacting fixed effects, and also a random intercept for epochs:

$$\begin{gathered} model = lmer(Accuracy \sim Epoch * Electrode\ number * Inverse\ solution \\ method * Connectivity\ measure + (1/Epoch)\ data = data) \end{gathered} \tag{9}$$

We applied a square root transform to the data, since this led to a better compliance of the model with the assumptions of normality and homoscedasticity of model's residuals than for raw data. Calculation of the significance of the fixed effects was performed using the Anova function of

bioRxiv preprint doi: https://doi.org/10.1101/2020.09.16.299305; this version posted September 16, 2020. The copyright holder for this preprint (which was not certified by peer review) is the author/funder, who has granted bioRxiv a license to display the preprint in perpetuity. It is made available under aCC-BY-NC-ND 4.0 International license.

the {*car}* package that computes F-tests (Fox and Weisberg, 2019). In order to assess the quality of the model, we computed marginal and conditional R^2 that were obtained from the {*MuMin*}package. In case of significant main effects, we performed *post-hoc* analyses using the *glht* function of the {*multcomp*} package that calculates adjusted p-values using individual z tests (Hothorn et al., 2008). The significance threshold was set to $p = 0.05$.

Results

As illustrated in Figure 2 and 3, the accuracy of the estimated networks was dramatically influenced by the density of scalp sensors. This influence was confirmed by the statistical analysis with a significant sensor density effect ($F_{(4,532)} = 361.94$, $p < 0.001$, $conditional\ R^2 = 0.84$, $marginal\ R^2 = 0.82$). The higher the number of electrodes, the more accurate the networks were. Post-hoc analyses showed significant accuracy improvement when using 256 electrodes (0.46, $sd = 0.32$) compared to 64 (0.24, $sd = 0.23$, $p < 0.05$), 32 (0.09, $sd = 0.08$, $p < 0.001$), and 19 (0.08, $sd = 0.08$, $p < 0.001$) electrodes. Increasing the sensor density from 128 electrodes to 256 electrodes did not provide further advantage ($p = 0.15$). A non-significant difference was obtained in all other cases. Differences between results obtained with 19 electrodes and those obtained with 32 ($p = 1$), 64 ($p = 0.93$), or 128 ($p = 0.47$) electrodes were all non-significant. Similarly, no differences were detected between 32 and 64 ($p = 0.85$), 32 and 128 ($p = 0.34$), 64 and 128 ($p = 0.92$) electrode montages. Regarding the inverse solution, wMNE (0.33, $sd = 0.33$) significantly outperformed eLORETA (0.15, $sd = 0.12$) ($F_{(1,532)} = 315.73$, $p < 0.001$, $conditional\ R^2 = 0.84$, $marginal\ R^2 = 0.82$).

bioRxiv preprint doi: https://doi.org/10.1101/2020.09.16.299305; this version posted September 16, 2020. The copyright holder for this preprint (which was not certified by peer review) is the author/funder, who has granted bioRxiv a license to display the preprint in perpetuity. It is made available under aCC-BY-NC-ND 4.0 International license.

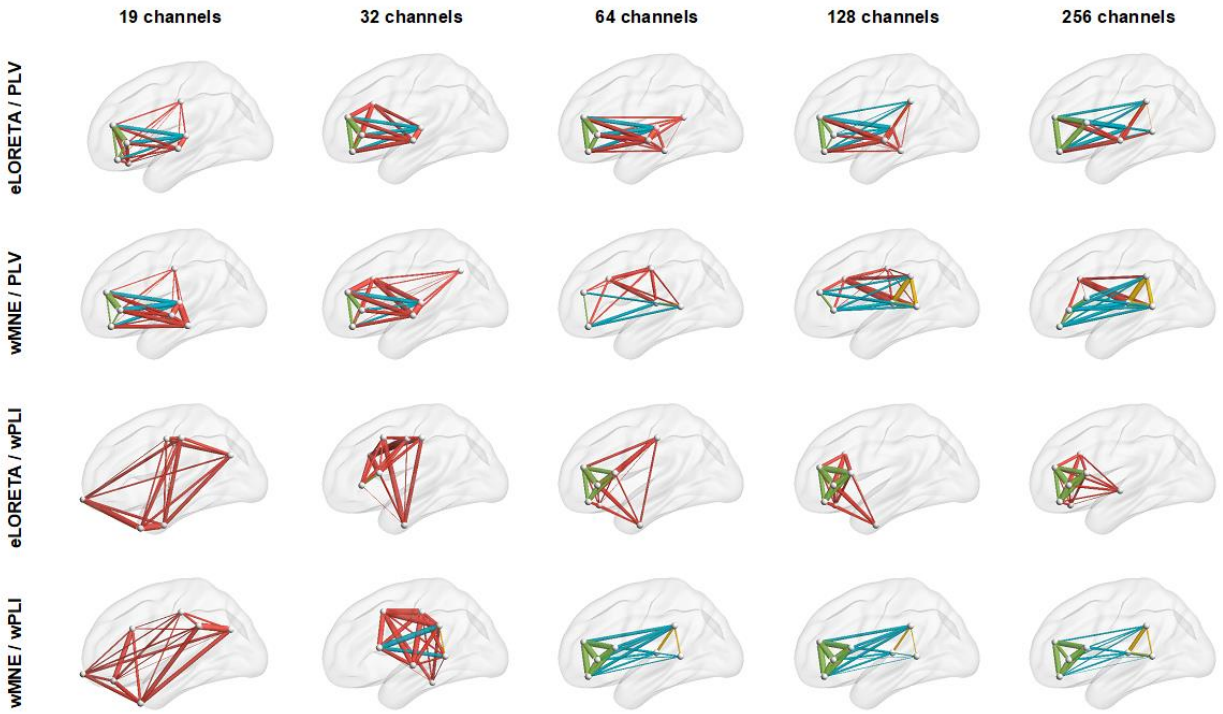

Fig. 2 Average networks over trials for all electrode montages and inverse solution/connectivity measure combinations. Connections in green and yellow belong to the epileptogenic and propagation subnetworks respectively. Connections in blue represent the connectivity between the two subnetworks. Connections in red are spurious connections, that do not exist in the reference network.

Also, statistical analyses showed a significant effect of the connectivity measure ($F_{(1,532)} = 99.35$, $p < 0.001$, $conditional\ R^2 = 0.84$, $marginal\ R^2 = 0.82$). The accuracy of the estimated networks was slightly higher with wPLI ($0.26, sd = 0.35$) than with PLV (0.23, $sd = 0.14$). Interestingly, the combination inverse solution/connectivity measure combination had also a significant effect on the network estimation accuracy ($F_{(1,532)} = 455.31$, $p < 0.001, conditional\ R^2 = 0.84, marginal\ R^2 = 0.82$).

bioRxiv preprint doi: https://doi.org/10.1101/2020.09.16.299305; this version posted September 16, 2020. The copyright holder for this preprint (which was not certified by peer review) is the author/funder, who has granted bioRxiv a license to display the preprint in perpetuity. It is made available under aCC-BY-NC-ND 4.0 International license.

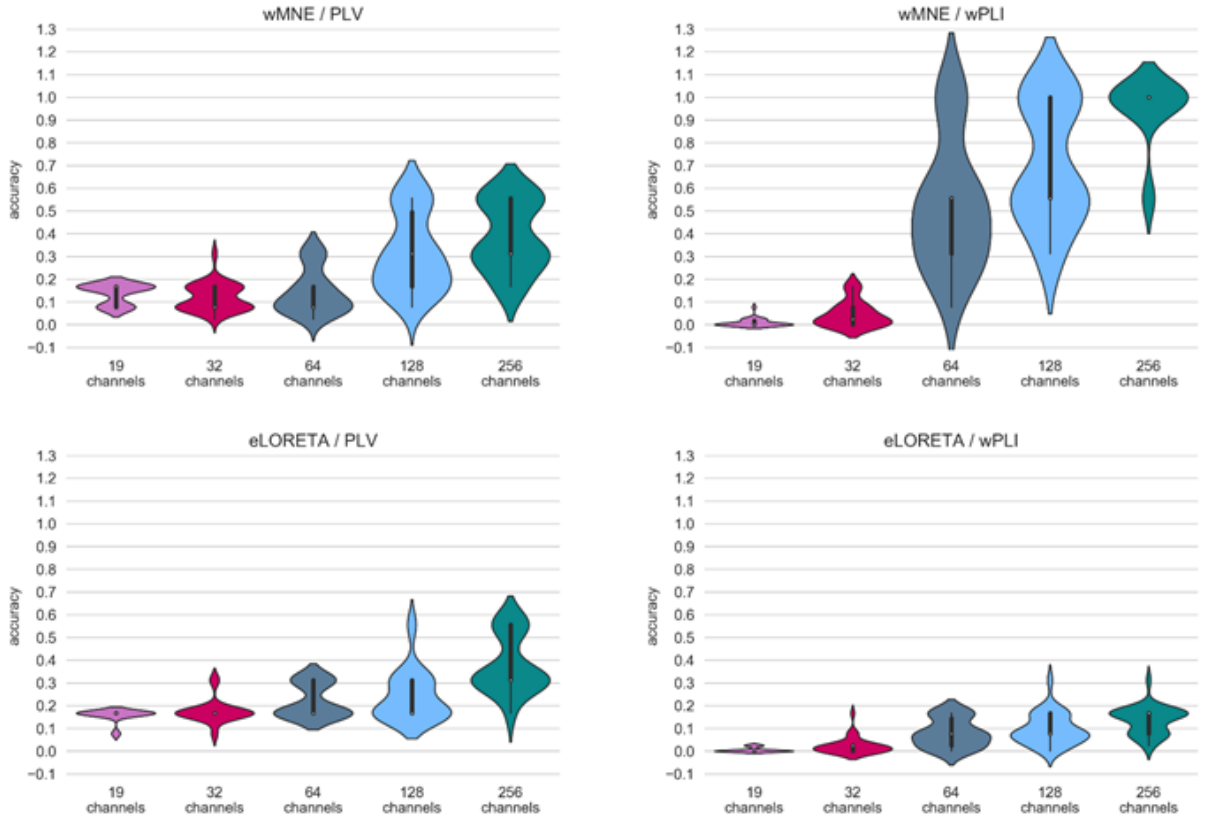

Fig. 3 Accuracy of the estimated based on different electrode montages for each inverse solution/connectivity measure. Values are ranged between 0 and 1.

bioRxiv preprint doi: https://doi.org/10.1101/2020.09.16.299305; this version posted September 16, 2020. The copyright holder for this preprint (which was not certified by peer review) is the author/funder, who has granted bioRxiv a license to display the preprint in perpetuity. It is made available under aCC-BY-NC-ND 4.0 International license.

The highest network estimation accuracy was reached using wMNE/wPLI $(0.44, sd = 0.41)$, while the worst performance was obtained with eLORETA/wPLI $(0.07, sd = 0.07)$. eLORETA/PLV $(0.23, sd = 0.11)$ and wMNE/PLV $(0.22, sd = 0.16)$ had similar average accuracy values. Post-hoc analyses showed significant difference between wMNE/wPLI and both eLORETA/PLV $(p < 0.001)$ and wMNE/PLV $(p < 0.001)$. Similarly, results obtained with eLORETA/wPLI were significantly different from those obtained with eLORETA/PLV $(p < 0.001)$ and wMNE/PLV $(p < 0.001)$. On the other hand, differences between eLORERA/PLV and wMNE/PLV $(p = 1)$ and between eLORETA/wPLI and wMNE/wPLI $(p = 0.98)$ were not statistically significant.

Discussion

To the best of our knowledge, there is still no consensus on the most optimized pipeline for reconstructing EEG source-space networks. At each step of this pipeline, several methods have indeed been proposed and many parameters need to be defined. Several comparative studies have investigated different methods/parameters affecting the estimation of functional networks. A key challenge in such studies (i.e. when dealing with real EEG data) is the absence of a ground truth, which prevents the exact evaluation of the performance of each considered method. In order to overcome this issue, we proposed to use in this paper a recently developed, physiologically-grounded computational model, and highlighted its potential use in optimizing the EEG network estimation procedure. Therefore, we used the model to simulate cortical-level sources from which scalp-EEG signals were generated, and also evaluated the effects of EEG channels density, two different source reconstruction algorithms, as well two different connectivity measures.

bioRxiv preprint doi: https://doi.org/10.1101/2020.09.16.299305; this version posted September 16, 2020. The copyright holder for this preprint (which was not certified by peer review) is the author/funder, who has granted bioRxiv a license to display the preprint in perpetuity. It is made available under aCC-BY-NC-ND 4.0 International license.

Overall, results obtained for the five considered electrode montages demonstrate clearly that the spatial resolution of the sensor array dramatically affects the accuracy of network estimation: as expected, increasing spatial resolution involves a higher accuracy of the reconstructed networks. These results were expected theoretically and are in line with previous studies (Lantz et al., 2003; Sohrabpour et al., 2015; Song et al., 2015). Recording EEG data with a low sensor density array could contribute to a misrepresentation of high spatial frequencies, and therefore high spatial resolution is required to avoid aliasing. Interestingly, increasing the number of electrodes from 128 to 256 did not provide significant improvement. On a different note, (Song et al., 2015) found that adding sensors on the inferior surface of the head (including the neck and the face) improves localization accuracy, even with sparse arrays. Therefore, it may be interesting to study the effect of the head coverage provided by different sensor array layouts, and not only the number of electrodes in each array.

Comparing inverse solutions and connectivity measures showed that wMNE performed better than eLORETA, and wPLI performed better than PLV. In contrast to our results, in (Tait et al., 2020), eLORETA outperformed wMNE at both voxel and ROI level. Even though (Colclough et al., 2016) did not recommend phase-based metrics as a first choice for assessing MEG functional connectivity, they, in general, favored using measures that are not affected by zero-lag phase coupling. Interestingly, our study showed that a more crucial parameter is the combination of inverse method and connectivity measure. Although wMNE/wPLI performed better than eLORETA/wPLI, the PLV connectivity measure performed similarly with both eLORETA and wMNE methods. Thus, the choice of the inverse solution and connectivity measure is recommended to be made simultaneously. In a previous study (Hassan et al., 2014), wMNE/PLV combination had the best performance in the context of a picture naming task. This combination has also showed better performance

bioRxiv preprint doi: https://doi.org/10.1101/2020.09.16.299305; this version posted September 16, 2020. The copyright holder for this preprint (which was not certified by peer review) is the author/funder, who has granted bioRxiv a license to display the preprint in perpetuity. It is made available under aCC-BY-NC-ND 4.0 International license.

than other combinations (eLORETA and wPLI were not included) when applied to simulated epileptic spikes (Hassan et al., 2017). A possible difference between the current simulations and (Hassan et al., 2017) is that, in the latter, the reference network were very dense locally with a very high number of zero-lag correlations which may favor methods that do not remove these connections (such as PLV). Moreover, neither eLORETA nor wPLI were investigated in that study. It is worth noting that the results obtained in this study are specific to the analyzed condition, i.e. epileptic spikes: therefore, we are not sure that the same combination of methods will show the best network estimation accuracy when analyzing networks related to cognitive tasks or resting state, such as the alpha/beta DMN for instance (i.e. physiological activity), which is the main objective of our further work.

Methodological considerations:

Here, our objective was to provide a typical example of the use of the COALIA model to investigate the effect of different pipeline-related parameters on EEG source-space network analysis. With our approach, we aimed at promoting the use of computational modeling as a ground-truth to evaluate parameters of EEG source connectivity methods. Using this approach, other parameters could be also evaluated and other scenarios could be also generated, and we suggest hereafter possible extensions for this work. First, we simulated in this study a network with 7 regions generating spike activity, while background brain activity was attributed to contributions from all other regions. However, it would be even more realistic for the network neuroscience field to use the model to simulate different rhythms of resting-state data (alpha/beta-band activity in the DMN network, for instance) and then evaluate the desired techniques in such context, rather than restricting the study to spikes/background activity scenarios. Second, the inverse solutions compared in this paper both belong to the family of minimum norm estimates methods. Other algorithms based on

bioRxiv preprint doi: https://doi.org/10.1101/2020.09.16.299305; this version posted September 16, 2020. The copyright holder for this preprint (which was not certified by peer review) is the author/funder, who has granted bioRxiv a license to display the preprint in perpetuity. It is made available under a CC-BY-NC-ND 4.0 International license.

beamformers, such as the widely used linearly constrained minimum variance (LCMV) were not tested here. Our choice was based on the results obtained in (Tait et al., 2020), where the use of LCMV methods for MEG source reconstruction was not recommended since it produces high localization error. It is worthy to mention that the two connectivity measures included in this study estimate phase synchrony between regional time-series. Other existing methods investigate instead the amplitude correlation between signals, such as the amplitude envelope correlation (AEC), which is widely used in the context of MEG functional connectivity. In a large study investigating the reliability of different connectivity metrics (Colclough et al., 2016), Colclough et al. have suggested that AEC between orthogonalized signals is the most consistent connectivity measure to employ in the context of resting-state recordings. Moreover, since we introduced a time delay between the two subnetworks, we propose that studying directional connectivity metrics (e.g., Granger causality) may also lead to additional insights. In order to threshold connectivity matrices, only the nodes with the highest 12% strength were kept, which was the value corresponding to the proportion of nodes originally used to simulate the 2 subnetworks. Obviously, this choice is not fully realistic, since we cannot have any *a priori* in experimental data on the exact number of activated brain regions. In addition, we used here the accuracy to quantify the difference between the estimated and reference networks. Other network-based metrics can be also useful to compute the similarities between these networks (Mheich et al., 2020, 2018). Finally, in order to make the simulations more realistic, several noise level could be also added to the scalp signals to mimic instrumental and measurement noises that occur in experimental settings.

Conclusion

In this work, we showed how COALIA, a recently developed, physiologically-inspired computational model can provide a ground-truth for comparative studies aiming at

bioRxiv preprint doi: https://doi.org/10.1101/2020.09.16.299305; this version posted September 16, 2020. The copyright holder for this preprint (which was not certified by peer review) is the author/funder, who has granted bioRxiv a license to display the preprint in perpetuity. It is made available under aCC-BY-NC-ND 4.0 International license.

optimizing the EEG-source connectivity pipeline. Using this model-based approach, several methodological questions could be addressed. Here, we assessed the effect of the number of EEG electrodes, as well as the inverse solution/connectivity measure combination. Our results suggest that a higher network estimation accuracy requires a high number of EEG electrodes and suggest the careful choice of an efficient inverse solution/connectivity measure combination.

Funding

This work was financed by the Rennes University, the Institute of Clinical Neuroscience of Rennes (project named EEGCog). It was also supported by the Programme Hubert Curien CEDRE (PROJECT No. 42257YA), the National Council for Scientific Research (CNRS-L) and the Agence Universitaire de la Francophonie (AUF) and the Lebanese university.

Conflicts of interest/Competing interest

The authors have no conflicts of interest to declare that are relevant to the content of this article.

Availability of data and material

Data used in this work can be found at https://github.com/sahar-allouch/BTOP-2020.git.

Code availability

COALIA model can be found at https://gitlab.com/yocmax/largescale. Data and Codes supporting the results of this study are available at https://github.com/sahar-allouch/BTOP-2020.git. We used Matlab (The Mathworks, USA, version 2018b), Brainstorm toolbox (Tadel et al., 2011), Fieldtrip toolbox (Oostenveld et al., 2011; http://fieldtriptoolbox.org),

bioRxiv preprint doi: https://doi.org/10.1101/2020.09.16.299305; this version posted September 16, 2020. The copyright holder for this preprint (which was not certified by peer review) is the author/funder, who has granted bioRxiv a license to display the preprint in perpetuity. It is made available under aCC-BY-NC-ND 4.0 International license.

OpenMEEG (Alexandre Gramfort et al., 2010) implemented in Brainstorm, and BrainNet Viewer (Xia et al., 2013).

Acknowledgments

This work was financed by the Rennes University, the Institute of Clinical Neuroscience of Rennes (project named EEGCog). Authors would also like to thank the Lebanese Association for Scientific Research (LASER) and Campus France, Programme Hubert Curien CEDRE (PROJECT No. 42257YA), for supporting this study. The authors would like to acknowledge the Lebanese National Council for Scientific Research (CNRS-L), the Agence Universitaire de la Francophonie (AUF) and the Lebanese university for granting Ms. Allouch a doctoral scholarship.

References

Alexandre Gramfort, Théodore Papadopoulo, Emmanuel Olivi, Maureen Clerc, 2010. OpenMEEG: opensource software for quasistatic bioelectromagnetics. BioMedical Engineering OnLine 9. https://doi.org/10.1186/1475-925X-8-1

Allen, E.A., Damaraju, E., Plis, S.M., Erhardt, E.B., Eichele, T., Calhoun, V.D., 2014. Tracking Whole-Brain Connectivity Dynamics in the Resting State. Cerebral Cortex 24, 663–676. https://doi.org/10.1093/cercor/bhs352

Anzolin, A., Presti, P., Van De Steen, F., Astolfi, L., Haufe, S., Marinazzo, D., 2019. Quantifying the Effect of Demixing Approaches on Directed Connectivity Estimated Between Reconstructed EEG Sources. Brain Topography. https://doi.org/10.1007/s10548-019-00705-z

Bartolomei, F., Guye, M., Wendling, F., 2013. Abnormal binding and disruption in large scale networks involved in human partial seizures. EPJ Nonlinear Biomedical Physics 1, 1–16. https://doi.org/10.1140/epjnbp11

Bassett, D.S., Sporns, O., 2017. Network neuroscience. Nature neuroscience 20, 353–364. https://doi.org/10.1038/nn.4502

Bates, D., Mächler, M., Bolker, B.M., Walker, S.C., 2015. Fitting linear mixed-effects models using lme4. Journal of Statistical Software 67. https://doi.org/10.18637/jss.v067.i01

Bensaid, S., Modolo, J., Merlet, I., Wendling, F., Benquet, P., 2019. COALIA: A Computational Model of Human EEG for Consciousness Research. Frontiers in Systems Neuroscience 13, 1–18. https://doi.org/10.3389/fnsys.2019.00059

Bradley, A., Yao, J., Dewald, J., Richter, C.P., 2016. Evaluation of electroencephalography source localization algorithms with multiple cortical sources. PLoS ONE 11, 1–14. https://doi.org/10.1371/journal.pone.0147266

Colclough, G.L., Woolrich, M.W., Tewarie, P.K., Brookes, M.J., Quinn, A.J., Smith, S.M., 2016. How reliable are MEG resting-state connectivity metrics? NeuroImage 138, 284–293. https://doi.org/10.1016/j.neuroimage.2016.05.070

bioRxiv preprint doi: https://doi.org/10.1101/2020.09.16.299305; this version posted September 16, 2020. The copyright holder for this preprint (which was not certified by peer review) is the author/funder, who has granted bioRxiv a license to display the preprint in perpetuity. It is made available under aCC-BY-NC-ND-4.0 International license.

Desikan, R.S., Ségonne, F., Fischl, B., Quinn, B.T., Dickerson, B.C., Blacker, D., Buckner, R.L., Dale, A.M., Maguire, R.P., Hyman, B.T., Albert, M.S., Killiany, R.J., 2006. An automated labeling system for subdividing the human cerebral cortex on MRI scans into gyral based regions of interest. NeuroImage 31, 968–980. https://doi.org/10.1016/j.neuroimage.2006.01.021

Fornito, A., Zalesky, A., Bullmore, E.T., 2010. Network scaling effects in graph analytic studies of human resting-state fMRI data. Frontiers in Systems Neuroscience 4, 1–16. https://doi.org/10.3389/fnsys.2010.00022

Fox, J., Weisberg, S., 2019. An R Companion to Applied Regression (Third). Sage. https://doi.org/10.1177/0049124105277200

Grova, C., Daunizeau, J., Lina, J.M., Bénar, C.G., Benali, H., Gotman, J., 2006. Evaluation of EEG localization methods using realistic simulations of interictal spikes. NeuroImage 29, 734–753. https://doi.org/10.1016/j.neuroimage.2005.08.053

Gueorguieva, R., Krystal, J.H., 2004. Move over ANOVA? Progress in Analyzing Repeated-Measures Data and Its Reflection in Papers Published in the Archives of General Psychiatry. Arch Gen Psychiatry 61, 310–317.

Halder, T., Talwar, S., Jaiswal, A.K., Banerjee, A., 2019. Quantitative evaluation in estimating sources underlying brain oscillations using current source density methods and beamformer approaches. eNeuro 6, 1–14. https://doi.org/10.1523/ENEURO.0170-19.2019

Hämäläinen, M.S., Ilmoniemi, R.J., 1994. Inetrpreting magnetic fields of the brain: minimum norm estimates. Medical & Biological Engineering & Computing 32, 35–42.

Hassan, M., Benquet, P., Biraben, A., Berrou, C., Dufor, O., Wendling, F., 2015. Dynamic reorganization of functional brain networks during picture naming. Cortex 73, 276–288. https://doi.org/10.1016/j.cortex.2015.08.019

Hassan, M., Dufor, O., Merlet, I., Berrou, C., Wendling, F., 2014. EEG source connectivity analysis: From dense array recordings to brain networks. PLoS ONE 9. https://doi.org/10.1371/journal.pone.0105041

Hassan, M., Merlet, I., Mheich, A., Kabbara, A., Biraben, A., Nica, A., Wendling, F., 2017. Identification of Interictal Epileptic Networks from Dense-EEG. Brain Topogr 30, 60–76. https://doi.org/10.1007/s10548-016-0517-z

Hassan, M., Wendling, F., 2018. Electroencephalography Source Connectivity. IEEE Signal Processing Magazine 81–96. https://doi.org/10.1109/MSP.2017.2777518

Hothorn, T., Bretz, F., Westfall, P., 2008. Simultaneous inference in general parametric models. Biometrical Journal 50, 346–363. https://doi.org/10.1002/bimj.200810425

Kabbara, A., Falou, W.E.L., Khalil, M., Wendling, F., Hassan, M., 2017. The dynamic functional core network of the human brain at rest 1–16. https://doi.org/10.1038/s41598-017-03420-6

Klem, G.H., Lüders, H.O., Jasper, H.H., Elger, C., 1999. The ten-twenty electrode system of the International Federation. The International Federation of Clinical Neurophysiology. Electroencephalogr. Clin. Neurophysiol. Suppl.

Lachaux, J.-P., Rodriguez, E., Le Van Quyen, M., Lutz, A., Martinerie, J., Varela, F.J., 2000. Studying Single-Trials of Phase Synchronous Activity in the Brain. International Journal of Bifurcation and Chaos 10, 2429–2439. https://doi.org/10.1142/s0218127400001560

Lantz, G., Grave de Peralta, R., Spinelli, L., Seeck, M., Michel, C.M., 2003. Epileptic source localization with high density EEG: How many electrodes are needed? Clinical Neurophysiology 114, 63–69. https://doi.org/10.1016/S1388-2457(02)00337-1

Mheich, A., Hassan, M., Khalil, M., Gripon, V., Dufor, O., Wendling, F., 2018. SimiNet: A Novel Method for Quantifying Brain Network Similarity. IEEE Transactions on Pattern Analysis and Machine Intelligence 40, 2238–2249. https://doi.org/10.1109/TPAMI.2017.2750160

Mheich, A., Wendling, F., Hassan, M., 2020. Brain network similarity: methods and applications. Network Neuroscience 4, 507–527.

O'Neill, G.C., Tewarie, P.K., Colclough, G.L., Gascoyne, L.E., Hunt, B.A.E., Morris, P.G., Woolrich, M.W., Brookes, M.J., 2016. Measurement of dynamic task related functional networks using MEG. NeuroImage. https://doi.org/10.1016/j.neuroimage.2016.08.061

bioRxiv preprint doi: https://doi.org/10.1101/2020.09.16.299305; this version posted September 16, 2020. The copyright holder for this preprint (which was not certified by peer review) is the author/funder, who has granted bioRxiv a license to display the preprint in perpetuity. It is made available under a CC-BY-NC-ND 4.0 International license.

Oostenveld, R., Fries, P., Maris, E., Schoffelen, J.-M., 2011. FieldTrip: Open Source Software for Advanced Analysis of MEG, EEG, and Invasive Electrophysiological Data. Computational Intelligence and Neuroscience 2011, 1–9. https://doi.org/10.1155/2011/156869

Pascual-Marqui, R.D., 2007. Discrete, 3D distributed, linear imaging methods of electric neuronal activity. Part 1: exact, zero error localization.

Schoffelen, J., Gross, J., 2009. Source Connectivity Analysis With MEG and EEG. Human Brain Mapping 30, 1857–1865. https://doi.org/10.1002/hbm.20745

Sohrabpour, A., Lu, Y., Kankirawatana, P., Blount, J., Kim, H., He, B., 2015. Effect of EEG electrode number on epileptic source localization in pediatric patients. Clinical Neurophysiology 126, 472–480. https://doi.org/10.1016/j.clinph.2014.05.038

Song, J., Davey, C., Poulsen, C., Luu, P., Turovets, S., Anderson, E., Li, K., Tucker, D., 2015. EEG source localization: Sensor density and head surface coverage. Journal of Neuroscience Methods 256, 9–21. https://doi.org/10.1016/j.jneumeth.2015.08.015

Stam, C.J., Nolte, G., Daffertshofer, A., 2007. Phase lag index: Assessment of functional connectivity from multi channel EEG and MEG with diminished bias from common sources. Human Brain Mapping 28, 1178–1193. https://doi.org/10.1002/hbm.20346

Tadel, F., Baillet, S., Mosher, J.C., Pantazis, D., Leahy, R.M., 2011. Brainstorm: A user-friendly application for MEG/EEG analysis. Computational Intelligence and Neuroscience 2011. https://doi.org/10.1155/2011/879716

Tait, L., Szul, M.J., Zhang, J., 2020. Cortical source imaging of resting-state MEG with a high resolution atlas : An evaluation of methods. https://doi.org/10.1101/2020.01.12.903302

Team, R.C., 2020. R: A Language and Environment for Statistical Computing. R Foundation for Statistical Computing, Vienna, Austria.

Vinck, M., Oostenveld, R., Van Wingerden, M., Battaglia, F., Pennartz, C.M.A., 2011. An improved index of phase-synchronization for electrophysiological data in the presence of volume-conduction, noise and sample-size bias. NeuroImage 55, 1548–1565. https://doi.org/10.1016/j.neuroimage.2011.01.055

Wang, H.E., Bénar, C.G., Quilichini, P.P., Friston, K.J., Jirsa, V.K., Bernard, C., 2014. A systematic framework for functional connectivity measures. Frontiers in Neuroscience 8. https://doi.org/10.3389/fnins.2014.00405

Wang, J., Wang, L., Zang, Y., Yang, H., Tang, H., Gong, Q., Chen, Z., Zhu, C., He, Y., 2009. Parcellation-dependent small-world brain functional networks: A resting-state fmri study. Human Brain Mapping 30, 1511–1523. https://doi.org/10.1002/hbm.20623

Wendling, F., Ansari-Asl, K., Bartolomei, F., Senhadji, L., 2009. From EEG signals to brain connectivity: A model-based evaluation of interdependence measures. Journal of Neuroscience Methods 183, 9–18. https://doi.org/10.1016/j.jneumeth.2009.04.021

Xia, M., Wang, J., He, Y., 2013. BrainNet Viewer: A Network Visualization Tool for Human Brain Connectomics. PLoS ONE 8, e68910. https://doi.org/10.1371/journal.pone.0068910

Zalesky, A., Fornito, A., Harding, I.H., Cocchi, L., Yücel, M., Pantelis, C., Bullmore, E.T., 2010. Whole-brain anatomical networks: Does the choice of nodes matter? NeuroImage 50, 970–983. https://doi.org/10.1016/j.neuroimage.2009.12.027